

A tomographic approach to inverse Mie particle characterization from scattered light

Jules S. Jaffe

Marine Physical Lab, Scripps Institution of Oceanography, University of California San Diego,
La Jolla, California, 92093-0238
jules@mpl.ucsd.edu

Abstract: The problem of computing the internal electromagnetic field of a homogeneous sphere from the observation of its scattered light field is explored. Using empirical observations it is shown that, to good approximation for low contrast objects, there is a simple Fourier relationship between a component of the internal E-field and the scattered light in a preferred plane. Based on this relationship an empirical algorithm is proposed to construct a spherically symmetric particle of approximately the same diameter as the original, homogeneous, one. The size parameter (ka) of this particle is then estimated and shown to be nearly identical to that of the original particle. The size parameter can then be combined with the integrated power of the scatter in the preferred plane to estimate refractive index. The estimated values are shown to be accurate in the presence of moderate noise for a class of size parameters.

© 2007 Optical Society of America

OCIS codes: 290.3200 (Inverse scattering); 290.4020 (Mie theory); 170.3010 (Image reconstruction techniques); 110.6960 (Tomography)

References and links

1. M. Born and E. Wolf, *Principles of Optics*, (Cambridge University Press, Seventh Edition, 2003).
2. M. I. Mishchenko, J. W. Hovenier and L. D. Travis, *Light Scattering by Nonspherical Particles*, (Academic Press, 2000).
3. P. J. Wyatt, "Differential Light Scattering: a Physical Method for Identifying Living Bacterial Cells," *Appl. Opt.* **7**, 1879-1896 (1968).
4. D. Carlton, and R. Kress, *Inverse Acoustic and Electromagnetic Scattering Theory*, (Springer-Verlag, Berlin, 1998).
5. P. C. Chaumet, K. Belkebir and A. Sentenac, "Three-dimensional sub wavelength optical imaging using the coupled dipole method," *Phys. Rev. B*, **69** (245405): 1-7 (2004).
6. A. C. Kak and M. Slaney, *Principles of Computerized Tomographic Imaging*, (Society of Industrial and Applied Mathematics, 2001).
7. V. V. Berdnik and V. A. Loiko, "Particle sizing by multiangle light-scattering data using the high-order neural networks," *J. Quant. Spectrosc. Radiat. Transfer* **100**, 55-63 (2006).
8. J. Everitt and I. K. Ludlow, "Particle sizing using methods of discrete Legendre analysis," *Biochem Soc. Trans.* **19**, 504-5 (1991).
9. K. A. Semyanov, P. A. Tarasov, A. E. Zharinov, A. V. Chernyshev, A. G. Hoekstra, and V. P. Maltsev, "Single-particle sizing from light scattering by spectral decomposition," *Appl. Opt.* **43**, 5110-5115 (2004).
10. P. H. Faye, "Spatial light-scattering analysis as a means of characterizing and classifying non-spherical particles," *Meas. Sci. Technol.* **9**, 141-149 (1998).
11. Y. L. Pan, K. B. Aptowicz, R. K. Chang, M. Hart, and J. D. Eversole, "Characterizing and monitoring aerosols by light scattering," *Opt. Lett.* **28**, 589-591 (2003).
12. B. Shao, J. S. Jaffe, M. Chachivili, and S. C. Esener, "Angular resolved light scattering for discriminating among marine picoplankton: modeling and experimental measurements," *Opt. Express* **14**, 12473-12484 (2006).
13. D. R. Bohren and D. R. Huffman, *Absorption and Scattering of Light by Small Particles*, Wiley-VCH, (1983).
14. H. C. Van de Hulst, *Light Scattering by Small Particles*, (Dover, 1981).
15. M. I. Mishchenko, L. D. Travis, and A. A. Lacis, *Scattering, Absorption, and Emission of Light by Small Particles*, (Cambridge University Press, Cambridge, 2002).

16. A. Taflove, *Computational Electrodynamics: The Finite-difference Time-domain Method*, (Artech House, Boston, MA, 1995).
17. B. T. Draine, "The Discrete-dipole approximation and its application to the interstellar graphite grains," *Astrophys. J.* **333**, 848-872 (1988).
18. B. T. Draine and P. J. Flatau, "Discrete-dipole approximation for scattering calculations," *J. Opt. Soc. Am.* **11**, 1491-1499 (1994).
19. I. K. Ludlow and J. Everitt, "Inverse Mie Problem," *J. Opt. Soc. Am. A.* **17**, 2229 – 2235 (2000).
20. T. L. Blundell and L. N. Johnson, *Protein Crystallography*, (Academic Press, 1976).
21. A. J. Devaney, "Inversion formula for inverse scattering within the Born approximation," *Opt. Lett.* **7**, 111-112 (1982).
22. A. C. Lavery, T. K. Stanton, D. E. McGehee, and D. Z. Chu, "Three-dimensional modeling of acoustic backscattering from fluid-like zooplankton," **111**, *J. Acous. Soc. Am.* 1197-1210 (2002).
23. P. L. D. Roberts and J. S. Jaffe, "Multiple angle acoustic classification of zooplankton," *J. Acous. Soc. Am.* **121**, 2060-2070 (2007).
24. H. R. Gordon, "Rayleigh-Gans scattering approximation: surprisingly useful for understanding backscatter from disk-like particles," *Opt. Express* **15**, 5572-5588 (2007).
25. A. Katz, A. Alimova, M. Xu, E. Rudolph, M. K. Shah, H. E. Savage, R. B. Rosen, S. A. McCormick and R. R. Alfano, "Bacteria Size Determination by Elastic Light Scattering," *IEEE J. Sel. Top. Quantum Electron.* **9**, 277-287 (2003).
26. A. Lompadó, "Light Scattering by a Spherical Particle," http://diogenes.iwt.uni-bremen.de/vt/laser/wriedt/Mie_Type_Codes/body_mie_type_codes.html
27. C. C. Dobson, and J. W. L. Lewis, "Survey of the Mie Problem Source Function," *J. Opt. Soc. Am. A* **6**, 463-466 (1989).
28. Q. Fu and W. Sun, "Mie theory for light scattering by a spherical particle in an absorbing medium," *Appl. Opt.* **9**, 1354-1361 (2001).
29. A. V. Oppenheim, R. W. Schaefer, and J. R. Buck, *Discrete-Time Signal Processing* A. V. Oppenheim, ed., (Prentice Hall Signal Processing Series, 1999) 2nd Edition.
30. C. Matzler, "Matlab codes for Mie Scattering and Absorption," http://diogenes.iwt.uni-bremen.de/vt/laser/wriedt/Mie_Type_Codes/body_mie_type_codes.html
31. W. Rysakov and M. Ston, "Light scattering by spheroids," *J. Quant. Spectrosc. Radiat. Transfer* **69**, 651-665 (2001).
32. V. M. Rysakov, "light scattering by "soft" particles of arbitrary shape and size: II-Arbitrary orientation of particles in the space," *J. Quant. Spectrosc. Radiat. Transfer* **98**, 85-100 (2006).
33. J. R. Fienup, "Phase retrieval algorithms: a comparison," *Appl. Opt.* **21**, 2758-2769 (1982).
34. L. M. Shulman, "Analysis of polarimetric data by solving the inverse scattering problem," *Quant. Spectrosc. Radiat. Transfer* **88**, 243-256 (2004).

1. Introduction

A long-standing problem in inverse optical electromagnetic theory has been the retrieval of the optical characteristics of a small particle from its scattered radiation field. Although the physics of the forward problem has been known for more than a century now [1] contemporary efforts have been focused on formulating a numerical framework for solving the forward problem of computing the scattered field from an object with arbitrary complex refractive index after irradiation by a plane wave [2]. The solution of the general inverse problem which consists of computing the 3-dimensionally varying particle's refractive index as a function of the scattered radiation had been envisioned many years ago [3], however it appears that progress in this area has been difficult and is likely due to the inherently ill-posed aspect of the task [4, 5].

In this article, the implementation of inverse diffraction tomography will be considered in context of inverting for the simplified case when the particle is homogeneous and spherical. Here, Mie theory provides an analytic formulation that can be used to predict both the internal and scattered fields that result from a plane wave incident upon a particle with radius a and complex index of refraction N_1 in a medium with refractive index N and hence, relative index of refraction of $m = \frac{N_1}{N}$. Although the ultimate goal of this work is aimed at a more general inverse, the problem is treated in this simplified context. As a guiding philosophy it is conjectured that if the inversion for particle characteristics here are found to be nearly impossible, it certainly portends ill for the more difficult case when arbitrary refractive index

and shape is desired. Fortunately, as described, in a class of relevant cases that have been numerically simulated, there exists a simple relationship between the internal electromagnetic field and the scattered radiation. This then permits the identification of the complex amplitude of the scattered field as values of the Fourier coefficients of the internal structure at a specific set of sinusoid waves via the far-field Fourier diffraction theory.

Next, taking advantage of this relationship, a simple algorithm is proposed for inverting for both particle size index and refractive index via inverse tomographic theory [6]. Although particle sizing in the context of Mie theory has been previously accomplished [7,8,9] the work described here demonstrates how inverse tomography theory can also be used to provide a working solution to this problem and moreover, provide a simple interpretation of the relationship between the scattered light and the particle's internal electric field.

Experimental motivation for this work is provided via the proliferation of optical scattering devices that are capable of the simultaneous observation of scatter over a multiplicity of angles [10,11]. As one application of this technology, we envision its use on single particles in order to identify oceanic microbes. Shao *et al.*, [12] demonstrated that bulk light scatter from several types of oceanic microbes have distinct patterns. The extension of these studies to permit additional knowledge of particle size, perhaps shape, and even the 3-dimensionally varying internal refractive index is an important eventual goal.

2. The forward electromagnetic scattering problem

As is well known, the most general physical framework for describing electromagnetic propagation is via Maxwell's equations [1]. In addition, the implementation of these equations to describe the scatter from "small particles" has been extensively studied [13, 14, 15].

Following [13], a suitable treatment starts by regarding the propagation of an incident plane wave along the z-axis in an orthonormal coordinate system with basis vectors $(\hat{e}_x, \hat{e}_y, \hat{e}_z)$. Defining the observed scattering direction as \hat{e}_r , a scattering plane can be defined as that plane that contains both the incident \hat{e}_i and the scattered vector \hat{e}_r . The incident electromagnetic field, assumed to be propagating along the z-axis has electric field \mathbf{E}_i that can be regarded as a superposition of components parallel and perpendicular to the scattering plane:

$$\mathbf{E}_i = (E_{0\parallel} \hat{e}_{\parallel i} + E_{0\perp} \hat{e}_{\perp i}) \exp(i k_{inc} z - i \omega t).$$

Here $k_{inc} = 2\pi N_1 / \lambda$ is the wave number in the internal medium, and λ is the wavelength of the incident light *in vacuo*.

At sufficiently large distances from the origin the scattered electromagnetic field is essentially transverse and can be represented as a superposition of two perpendicular vector components that are defined in terms of the scattering plane and the direction of propagation as

$$\mathbf{E}_s = E_{\parallel s} \hat{e}_{\parallel s} + E_{\perp s} \hat{e}_{\perp s}$$

where $\hat{e}_{\parallel s} = \hat{e}_\theta$, $\hat{e}_{\perp s} = -\hat{e}_\phi$, $\hat{e}_{\perp s} \times \hat{e}_{\parallel s} = \hat{e}_r$.

Here, (r, θ, ϕ) are defined in terms of a conventional spherical coordinate system relative to the scattering plane and the direction of propagation. This notation permits the relation between incident and scattered fields to be written (omitting the time dependence) in compact matrix form as

$$\begin{pmatrix} E_{\parallel s} \\ E_{\perp s} \end{pmatrix} = \frac{\exp ik(r-z)}{-ikr} \begin{pmatrix} S_2 & S_3 \\ S_4 & S_1 \end{pmatrix} \begin{pmatrix} E_{\parallel i} \\ E_{\perp i} \end{pmatrix} \quad (1)$$

As noted in [13] the incident and scattered light are considered relative to different basis vectors. In addition, the values of the amplitude scattering matrix “S” are complex and generally a function of the spherical coordinates θ and ϕ .

In the most general case, there are no closed form solutions to compute the scatter from an arbitrary particle. Rather, one needs to use a numerical model to predict \mathbf{E}_s [2]. Examples are the T-Matrix [15], the use of FDTD [16] methods as well as the Discrete Dipole Approximation [17].

Considerable simplifications can be made in the case that the particle is spherical and homogeneous. This is the celebrated and rigorous case of Mie theory where a closed form solution can be prescribed. To start, consider an electric field vector propagating along the z-axis with the polarization constrained to lie along the x-axis. Such a field can be represented as $\mathbf{E}_i = E_0 \exp^{ikr \cos \theta} \hat{\mathbf{e}}_x$.

The scatter from this particle can be found by expanding the incident, internal, and scattered electric fields into spherical harmonics. The incident wave can be represented as

$$\mathbf{E}_i = E_0 \sum_{n=1}^{\infty} i^n \frac{2n+1}{n(n+1)} (\mathbf{M}_{o\ln}^{(1)} - i \mathbf{N}_{e\ln}^{(1)}), \quad (2)$$

the internal electric field by

$$\mathbf{E}_{\text{int}} = E_0 \sum_{n=1}^{\infty} i^n \frac{2n+1}{n(n+1)} (c_n \mathbf{M}_{o\ln}^{(1)} - id_n \mathbf{N}_{e\ln}^{(1)}), \quad (3)$$

and the scattered field by

$$\mathbf{E}_s = E_0 \sum_{n=1}^{\infty} i^n \frac{2n+1}{n(n+1)} (ib_n \mathbf{N}_{o\ln}^{(3)} - a_n \mathbf{M}_{e\ln}^{(3)}), \quad (4)$$

where the corresponding vector spherical harmonics are defined as

$$\mathbf{M}_{o\ln} = \cos \phi \pi_n(\cos \theta) z_n(\rho) \hat{\mathbf{e}}_\theta - \sin \phi \tau_n(\cos \theta) z_n(\rho) \hat{\mathbf{e}}_\phi,$$

$$\mathbf{M}_{e\ln} = -\sin \phi \pi_n(\cos \theta) z_n(\rho) \hat{\mathbf{e}}_\theta - \cos \phi \tau_n(\cos \theta) z_n(\rho) \hat{\mathbf{e}}_\phi,$$

$$\begin{aligned} \mathbf{N}_{o\ln} = & \sin \phi n(n+1) \sin \theta \pi_n(\cos \theta) \frac{z_n(\rho)}{\rho} \hat{\mathbf{e}}_r + \sin \phi \tau_n(\cos \theta) \frac{[\rho z_n(\rho)]'}{\rho} \hat{\mathbf{e}}_\theta \\ & + \cos \phi \pi_n(\cos \theta) \frac{[\rho z_n(\rho)]'}{\rho} \hat{\mathbf{e}}_\phi, \end{aligned}$$

$$\begin{aligned} \mathbf{N}_{e\ln} = & \cos \phi n(n+1) \sin \theta \pi_n(\cos \theta) \frac{z_n(\rho)}{\rho} \hat{\mathbf{e}}_r + \cos \phi \tau_n(\cos \theta) \frac{[\rho z_n(\rho)]'}{\rho} \hat{\mathbf{e}}_\theta \\ & - \sin \phi \pi_n(\cos \theta) \frac{[\rho z_n(\rho)]'}{\rho} \hat{\mathbf{e}}_\phi. \end{aligned}$$

The functions z_n with $n = 1$ denotes the spherical Bessel function $j_n(k_1 r)$ and with $n = 3$ the spherical Hankel function $h_n^{(1)}(kr)$. The functions π_n and τ_n are derived from the Legendre

polynomials P_n via the relationships $\pi_n = \frac{P_n^1}{\sin \theta}$, $\tau_n = \frac{dP_n^1}{d\theta}$. A more complete discussion is covered in [13], whose notation has been adopted.

A further simplification of Eq. (1) can be obtained by enforcing the requirement that the radial component of the electric field goes to zero at large distances. This results in

$$\begin{pmatrix} E_{\parallel s} \\ E_{\perp s} \end{pmatrix} = \frac{\exp^{ik(r-z)}}{-ikr} \begin{pmatrix} S_2 & 0 \\ 0 & S_1 \end{pmatrix} \begin{pmatrix} E_{\parallel i} \\ E_{\perp i} \end{pmatrix}. \quad (5)$$

Casting these equations back into Cartesian coordinates, we note that if the incident electric field is polarized along the x-axis and the light is observed in the y-z plane, this implies that $E_{\perp i} = E_x$ and $E_{\parallel i} = 0$ whereby $E_{\parallel s}(0, y, z) = 0$ and $E_{\perp s} = S_1 E_{\perp i} = S_1 E_x$. As such, pure S_1 can be observed in the y-z plane as there is no incident parallel component in this case. Observations in the x-y plane can be similarly viewed as pure S_2 as there is no perpendicular component.

A view of the internal electromagnetic field and its far field is facilitated via envisioning the radiated field as due to the radiation from a superposition of internal dipoles. Consider now the relationship between a set of N dipoles at locations r_j with polarizations \mathbf{P}_j due to the electric field \mathbf{E}_j where $\mathbf{E}_j = \alpha_j \mathbf{P}_j$ and α is the polarizability of the medium at these locations [18]. The field far field due to these dipoles can then be computed at the position of vector \mathbf{d} with unit vector $\hat{\mathbf{d}}$ and magnitude d as a superposition of individual fields as

$$\mathbf{E}_s(\mathbf{d}) = \frac{k^2 \exp(ikd)}{d} \sum_{j=1}^N \exp(-ik \hat{\mathbf{d}} \cdot \mathbf{r}_j) (\hat{\mathbf{d}}\hat{\mathbf{d}} - \mathbf{1}_3) \mathbf{P}_j. \quad (6)$$

Note that wave number k here refers to the medium. Considering now the observation of this scattered light on a sphere of radius |d| in direction $\mathbf{k}_{\text{obs}} = (k_{ox}, k_{oy}, k_{oz})$, centered on the spherical particle so that $\hat{\mathbf{k}}_{\text{obs}} = \hat{\mathbf{d}}$, this equation can be rewritten as

$$\mathbf{E}_s(\hat{\mathbf{k}}_{\text{obs}} \mathbf{d}) = \frac{k^2 \exp(ikd)}{d} \sum_{j=1}^N \exp(-ik \hat{\mathbf{k}}_{\text{obs}} \cdot \mathbf{r}_j) (\hat{\mathbf{k}}_{\text{obs}} \hat{\mathbf{k}}_{\text{obs}} - \mathbf{1}_3) \mathbf{P}_j. \quad (7)$$

Assuming now that the data is observed in the y-z plane so that $\mathbf{k}_{\text{obs}} = (0, k_{oy}, k_{oz})$, and that the d distance is implicit in the treatment the x component of this sum can be written as

$$E_{sx}(\hat{\mathbf{k}}_{\text{obs}}) = \frac{k^2 \exp(ikd)}{d} \sum_{j=1}^N \exp(-ik_{\text{obs}} \cdot \mathbf{r}_j) (-\mathbf{P}_{jx}). \quad (8)$$

Assuming that the matrix α is diagonal, and does not depend on location “j”, because the sphere is homogeneous, one can substitute $\mathbf{P}_{jx} = \frac{E_{x\text{-int}}}{\alpha}$ to obtain the observed x component of the electric field in the direction \mathbf{k}_{obs}

$$E_{sx}(\mathbf{k}_{\text{obs}}) = \frac{k^2 \exp(ikd)}{d \alpha} \sum_{j=1}^N -E_{x\text{-int}}(\mathbf{r}_j) \exp(-ik_{\text{obs}} \cdot \mathbf{r}_j). \quad (9)$$

This can be identified as the Fourier Transform of the x-component of the electric field, evaluated at spatial wave number $\mathbf{k}_{\text{obs}} = (k_{oy}, k_{oz})$ multiplied by the constant phase and

amplitude factor $\frac{k^2 \exp(ikd)}{d\alpha}$. Note that in the y-z plane $E_{s\perp} = E_{sx}$ and also since $E_{s\parallel} = E_{sy} + E_{sz} = 0$, it implies that $E_{sy} = 0$ and $E_{sz} = 0$.

3. The inverse electromagnetic scattering problem

3.1 Inverse Mie theory

Using the framework described above, the inverse Mie problem can be simply stated as: *Given the amplitude scattering functions S_1 and S_2 , invert for radius “a” and refractive index N_1 .*

In consideration of work accomplished by other researchers, one set of approaches that can be described as “empirical” decomposes the scattered radiation into a set of orthogonal polynomials that are then used to achieve classification [8]. Another method used neural nets to obtain particle characteristics via training the net on synthetic data [7]. Another method, more akin to that proposed here, used spectral analysis of the scattered data. [9].

One approach based on the analytic form of the Mie theory equations [19] demonstrated that the Mie coefficients a_n and b_n can be obtained from the scattered data using the integral relationships:

$$a_n = \frac{1}{2n(n+1)} \int_0^\pi [S_{\parallel}(\theta)\tau_n(\theta) + S_{\perp}(\theta)\pi_n(\theta)] \sin \theta d\theta. \quad (10)$$

$$b_n = \frac{1}{2n(n+1)} \int_0^\pi [S_{\parallel}(\theta)\pi_n(\theta) + S_{\perp}(\theta)\tau_n(\theta)] \sin \theta d\theta. \quad (11)$$

Once these coefficients are known, a back projected version of the scattered field can be plotted against various radii in order to obtain an estimate of the particle size and also the refractive index of the particle in the absence of attenuation. The authors show that the procedure produces a unique value for particle radius and refractive index from consideration of the analytic properties of the Mie theory equations.

3.2 Diffraction tomography

Computerized tomography and its variants have been in use for quite some time. The most traditional field utilizing these methods is that of x-ray crystallography where the retrieval of the 3-dimensional structure of molecules has now become routine if high quality crystals are available. The method consists of the use of lens-less imaging where the diffraction pattern of various forms of a specimen are observed in order to infer the phase of the object in addition to the measured amplitudes of the Fourier coefficients which are readily deduced from the measured intensities [20]. A necessary condition for the inversion to work is that the object itself does not substantially perturb the incident field so that the internal field is primarily due to the incident wave. This is the case of the Born approximation [1].

A further variant of the Born approximation called the Distorted Wave Born Approximation (DWBA) considers the change in the phase velocity of the wave due to the internal structure of the particle. Here, it is again assumed that the internal field can be simply related to the incident one. As described in [21], the spatially varying internal refractive index can be estimated via inversion of the formula

$$f_{scat} = \frac{k^2}{4\pi} \iiint_V N(r) e^{i(\mathbf{k}_{scat} - \mathbf{k}_{inc}) \cdot \mathbf{r}_v} dV. \quad (12)$$

Here k is the wave number of the incident radiation and the subscript “2i” refers to the fact that the wave number of the wave vector k is evaluated in the interior of the volume. The variable \mathbf{r}_v is the position vector of any volume element within the specimen volume V . The DWBA has been successfully used in a number of areas to provide a simplified option for formulating scatter [22]. Using this relationship, inverse techniques have been proposed for classifying organisms [23].

Considering now the application of these methods to the problem of inverting for particle characteristics from light scatter it is certainly an open issue as to how “weak” a scatterer can be and still conform to either of these assumptions. As one application of the Born approximation, one can use Rayleigh Gans (RG) theory in order to interpret their scatter. The conditions for this theory to be true, referred to by [13] as being *heuristic*, are well known and usually imply that both $|m - 1| \ll 1$ and $kd|m - 1| \ll 1$. Here d is some characteristic dimension of the particle and k is the wave number, presumably inside the object. Although this theory has proven useful in some situations [24, 25], its restrictive nature would seem to limit its range of application to very small particles.

Consider now the simplification that can be imposed upon Eq. (9) when the x-component of the internal E field is related to the phase of the incident wave field so that x-component of the internally generated field, E_{x-int} can be represented as

$$E_{x-int} = E_x(\mathbf{r}_j) \exp(i\mathbf{k}_{inc} \cdot \mathbf{r}_j). \quad (13)$$

The wave number \mathbf{k}_{inc} is taken to be that of the interior. In this case, the observed complex scattering coefficients can be rewritten as

$$E_{xs}(\mathbf{k}_{obs}) = \frac{k^2 \exp(ikd)}{d\alpha} \sum_{j=1}^N E_{x-int}(\mathbf{r}_j) \exp(-i(\mathbf{k}_{obs} - \mathbf{k}_{inc})_{int} \cdot \mathbf{r}_j) \quad (14)$$

where the subscript on the wave number inside the sum refers to the particle interior. Assuming that $|\mathbf{k}_{obs}| \cong |\mathbf{k}_{inc}|$, a geometric interpretation of this expression is that the complex Fourier coefficients of the internal E_x field are measured at locations \mathbf{k}_{obs} on a circle of radius $|k| = 2\pi/\lambda$ centered at $-\mathbf{k}_{inc}$. These observed coefficients can then be related to the wave number inside the particle evaluated at $\mathbf{k}_{struc} = \mathbf{k}_{obs} - \mathbf{k}_{inc}$. Figure 1 illustrates the relationship. The formulation is almost identical to that considered before as in Eq. (12), except in this case we are solving for the internal electric field instead of a physical characteristic of the particle. Using compact notation so that \mathbb{F} corresponds to taking a Fourier transform, (14) can be written as $E_{xs}(\mathbf{k}_{obs}) \propto \mathbb{F}(E_{x-int})$ where the transform is evaluated on a circle at locations $\mathbf{k}_{obs} - \mathbf{k}_{inc}$. Note that this relationship is only true for the x component of the interior electric field when the incident radiation is polarized along the x-axis and where the scattered light is observed in the y-z plane for a homogeneous sphere.

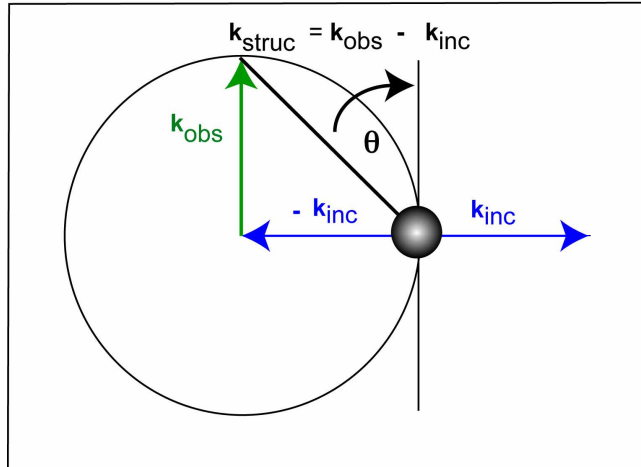


Fig. 1. The observed complex angular light scattered data can be viewed as the coefficients of the Fourier Transform of the structure: $\mathbb{F}(k_{struc})$ on the Ewald sphere [20] that is centered $-k_{inc}$ at a radius of $|k| = 2\pi/\lambda$.

4. Numerical simulations to investigate the linear phase assumption via Mie theory.

Based on the goals as described above, a numerical implementation of Mie theory was undertaken in order to determine whether, in this well understood case, an empirical relationships could be established between the internal electric field and the scattered light. In the case of a weak scatterer, as summarized above, a straightforward relationship exists between the internal structure and its Fourier Transform. However in the case of electromagnetic waves it is well known that the interior field of a particle is a sum of the radiation from the incident field and other parts of the structure. This is an important consideration in the Discrete Dipole Approximation [DDA] where, in Eq. (3) above, the electric field is due to a superposition of the incident field and contributions from the other dipoles. Here, since Mie theory is analytically correct and readily numerically implemented it seemed prudent to examine this simplified case before going on to arbitrary particle shapes and internal structures.

As such, Mie theory was implemented in Mathematica [Wolfram, IL] using the equations listed above. A preliminary version of this program was obtained from [26] authored by A. Lompadó. The program was checked for correctness by extensive examination of the code and by comparing the results of the simulations with other published results [27, 28]. A necessary detail of the simulations was to determine how many terms were needed in the linear sum in Eqs. (2), (3). Here, an empirical approach was taken in that the series values were examined to insure that the addition of more terms led to a very small change in the summation. A value of .001 fractional change was considered to be adequate.

As two applications of the proposed methodology simulations were performed on relative refractive indices that would correspond to a small cell or marine microbe suspended in saline solution $m = (1.38/1.338) \sim 1.035$ and a bacteria suspended in air: $m = 1.58/1.00 = 1.58$. A nominal value for the complex attenuation coefficient was used, .001. Particle radii of .25, .5, 1, 2, and 4 μm were used with an incident light wavelength of .5 μm . The size parameters for these particles are therefore $= \pi, 2\pi, 4\pi, 8\pi,$ and 16π .

The data were analyzed to see if the internal electric field could be interpreted in the context of a weak object. Since previous results indicated that the amplitude of this internal field was not constant, even for a low contrast object, efforts were focused on examining the

data to see if the internal field was at least linear in a phase relationship that was dictated by the internal refractive index. Specifically we sought to identify whether the internal E_{x-int} field could be approximated by $E_{x-int} = E_x(\mathbf{r})\exp(ik_z z)$. We refer to this assumption as a Reduced Distorted Wave Born Approximation (RDWBA) as the assumption of an internal field with linear phase is more general than the DWBA. This was accomplished by simply examining the z -dependent phase and noting its linearity as well as by computing the standard deviation of the superposition of all of the z dependent phases at a given z coordinate as a function of particle size and contrast for the particles.

Figure 2 shows two graphs of the phase of the internal E_x field along the z -axis for the two cases where $(a, m) = (1 \mu\text{m}, 1.05)$ and $(1 \mu\text{m}, 1.58)$. The graph depicts this phase for a lattice of 21 points as a function of the z dependence where the error bars denote one standard deviation. Note that the graphs span the range of phases from $-\pi$ to π so that the phase wraps. The results indicate that a linear phase assumption for the E_x field is clearly warranted in the lower contrast case. This was true in all of the lower contrast cases. This is certainly not true in the higher contrast case and was also found to be unreasonable in all of the higher contrast ones.

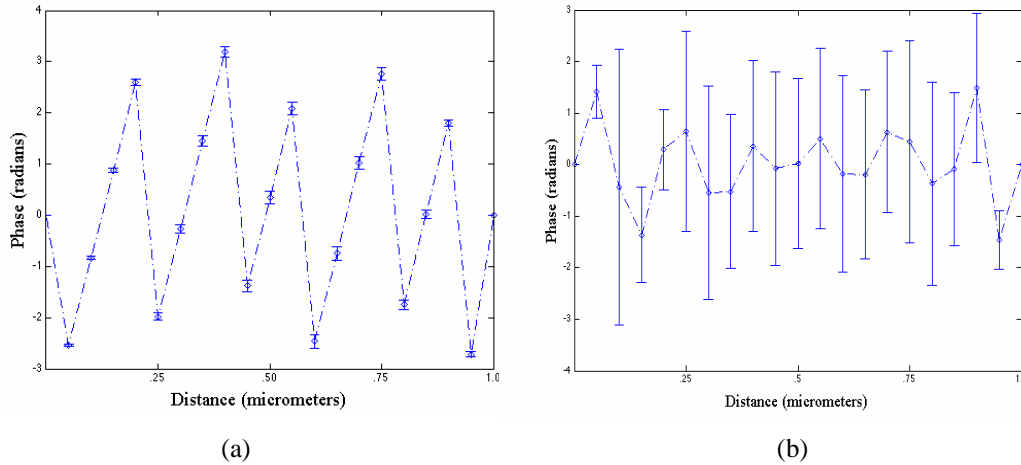


Fig. 2. Two graphs of the phase of the internal E_x field along the z -axis for the cases where $(a, m) = (1 \mu\text{m}, 1.05)$ (a) or $(1 \mu\text{m}, 1.58)$ (b). The graph depicts a superposition of the z -dependent phase along with the standard deviation of those phases at a given z location. Graphs were produced via the implementation of Mie theory to compute the interior electric field for a spherical particle embedded inside a cubic lattice of dimensions $(21)^3$.

5. A proposed algorithm for particle size and refractive index estimation

5.1 Motivation

Given now that the S_1 scattering amplitudes can be related to the Fourier coefficients of E_{x-int} , the potential of using this information to estimate particle size and refractive index was investigated. As one approach, a spherically symmetric particle can be constructed from these values by filling in the remainder of 3-dimensional Fourier Space so that $E_x(|k|) = E_{x,obs}(|\mathbf{k}_{obs}|)$ where the italic notation implies that $E_x(|k|) = \mathbb{F}(E_{x-int}(|\mathbf{k}_{obs}|))$. Simply stated, the algorithm takes the Fourier coefficient observed at wave number \mathbf{k}_{obs} , identifies it as corresponding to the internal wave number of the electric field structure at $\mathbf{k}_{struc} = \mathbf{k}_{obs} - \mathbf{k}_{inc}$ and then uses this value to create a 3-dimensional particle whose Fourier Transform has this coefficient at all locations of radius $|\mathbf{k}_{struc}|$. The inverse Fourier transform

of this spherically symmetric function is also a spherically symmetric real space structure. The size parameter of this object is then estimated via comparison with other objects of known size parameter.

Given this proposed algorithm, there are a myriad of issues related to its underlying assumptions and potential performance. One approach, taken here, evaluates the performance of the algorithm via simulations. Assuming that the internal x-component of the E field can be represented as a constant offset (DC term) plus some smaller fluctuations, via the linearity of the Fourier Transform, the Fourier Transform of this object consists of the Fourier transform of the DC term plus the Fourier Transform of the smaller fluctuations. If the DC term dominates the real space structure, the estimated radius of this spherically symmetric particle will be close to the particle's true radius.

Next, assuming that an estimate for the size parameter is available, a means for estimating refractive index would be useful. This could then be used to estimate absolute size. A simple approach taken here is to use the integrated power in the S1 component in concert with the size parameter to estimate refractive index. For low contrast ($m < 1.2$) and relatively small particles (size index $< 4\pi$) the integrated power in the S1 component is monotonically increasing as a function of size index. A simple look up table can then be used to combine both the size index and the integrated power to estimate refractive index and hence size.

5.2 The numerical implementation of the algorithm

In this section we discuss some aspects of the numerical implementation of the algorithm. In order to estimate the size parameter a variant of the procedure for simply interpolating wave number in Fourier space and then performing an inverse 3-dimensional transform was used. This is because the simple interpolation scheme did not lead to good results, even for test data where a homogeneous spherical particle was simulated. Instead, the values of the observed angular scatter, corresponding to the Fourier Transform of the structure obtained as explained above, were interpolated onto a radial spoke in Fourier space. This was then Inverse Fourier Transformed to produce a doubly projected real space structure. By doubly projected what is meant is that the 3-dimensional real space structure is integrated first along one of the principle axes and then along another one to produce a one-dimensional function. Define the Fourier Transform as

$$\mathbb{F}(\mathbf{s}) = \iiint_V \mathbf{E}_x(\mathbf{r}) e^{-2\pi i \mathbf{r} \cdot \mathbf{s}} dx dy dz,$$

where the \mathbf{r} vector can be written as (x,y,z) and the \mathbf{s} vector as (s_x, s_y, s_z) . Evaluating the Fourier Transform along the s_x axis leads to

$$\mathbb{F}(s_x, 0, 0) = \int \left[\iiint_V \mathbf{E}_x(\mathbf{r}) dy dz \right] e^{-2\pi i x s_x} dx = \int E_{p_x}(x) e^{-2\pi i x s_x} dx,$$

where $E_{p_x}(x) = \iiint_V \mathbf{E}_x(\mathbf{r}) dy dz$. This implies that the values of the Fourier Transform on the line defined by $F(s_x, 0, 0)$ can be viewed as the one dimensional Fourier Transform of the doubly projected structure $E_x(\mathbf{r})$. Via the uniqueness of the Fourier relationship this then implies that $E_x(\mathbf{r})$ can be retrieved from $\mathbb{F}(s_x, 0, 0)$ via an Inverse Fourier Transform. However, since this function has been assumed to be spherically symmetric, any line through the origin of Fourier space will do. The algorithm therefore takes an inverse transform of $\mathbb{F}(s_x, 0, 0)$ in order to estimate $E_{p_x}(x) = \iiint_V \mathbf{E}_x(\mathbf{r}) dy dz$ and then uses an Inverse Radon Transform (doubly implemented) to compute a two dimensional slice through the spherically

symmetric function $E_x(|\mathbf{r}|)$. The above discussion defines the “projection slice theorem” that is the basis for most tomographic theory in this linear case. These algorithms are standard now and good explanations of how they work can be found in several texts [6].

In order to test the proposed algorithm for reconstructing a spherically symmetric object from a radial spoke of its Fourier Transform numerical experiments were implemented on homogeneous 3-dimensional spheres. The procedure took 1-dimensional Fourier Transforms of doubly projected versions of homogeneous spheres, interpolated this data onto the Fourier coefficients sampled by the S_1 amplitude function, and then performed an inversion of this procedure to obtain an image of a slice through the 3-dimensional particle. Excellent reconstruction of homogeneous spheres resulted from this procedure. The Inverse Radon Transform was implemented in MATLAB (Mathworks, MA) using the “iradon” function as was all of the numerical studies at this stage.

The particle size parameter was then estimated using standard signal processing methods [29] via maximization of the cross correlation of the 2-dimensional slice through the 3-dimensional object with a set of 2-dimensional disks of varying radii. Values of the cross-correlation output were inspected for both accuracy and to characterize the shape of the peak.

5.3 Numerical results

Numerical experiments were performed in order to compute the S_1 function and to implement the inverse Mie algorithm as described above. The Mie code used was available as freeware [30] and was validated via comparison with an F77 program [13] for a select number of cases.

For the simulations, the set of particle sizes and refractive indices used were the same as above, that is, size indices of π , 2π , 4π , 8π , and 16π . In order to examine the sensitivity of the data inversion technique 10% noise was added to the real and imaginary components of the simulate observed angular scattered data. Multiplicative noise was chosen here because the dynamic range of the scattered values are extremely high and in practice some type of variable density filter would be used to prefilter the light and reduce the dynamic range of the data. The light incident on a photo detector would therefore be attenuated as a function of angle. Receiver noise would then be added to this attenuated light. The main purpose of adding noise here was to explore whether the numerical implementation of the algorithm was extremely sensitive as is the case when inversions are ill posed. No claims are made that this value mimics what a real world detector would see but rather it is just a first step in looking at the broader issues of stability. Results for the estimated size parameters for the simulated particles are shown in Tables 1 for the index of refraction $m = 1.035 + .001i$.

Table 1. Averages and standard deviations of retrieved values for the size index when $m = 1.035 + 0.001i$. The data was obtained by performing 100 repeated tomographic inversions after 10% multiplicative noise was added to the real and imaginary parts of the simulated complex angular scatter.

Particle size index	3.14	6.28	12.56	25.13	50.27
Retrieved size index	2.78	6.34	12.50	25.47	52.25
Standard deviation	0.02	<0.	0.07	0.06	0.1
Approximate % Error	12	1	5	1	4

The results of this inverse procedure indicate that for the low contrast particles ($m = 1.035 + .001i$), the size index can be estimated quite well. This was expected based on the fact that internal field is quite linear in phase. Tests were also performed with the set of higher index

of refraction particles ($m = 1.58 + .001i$) and did not lead to accurate estimates of size index nor high values for cross correlation.

The next step was to use the size index data in order to examine the capability to estimate particle refractive index. In order to achieve this, a precomputed look up table was created that listed the total power in the measured S_1 component as a function of size and refractive index using the Mie model. This provided a reference data set. Next, given the values of the size index a set of noisy complex angular scatter data was produced as above. An estimate of refractive index was then obtained by computing the closest index of refraction for the given size index that was experimentally obtained (as listed in Table 1) and the predicted, noisy, observed power estimate from the simulated S_1 component. This was done 100 times for each size class and the average and standard deviation for the refractive index were computed. The values are listed in Table 2.

Table 2. Averages and standard deviations of retrieved values of the refractive index for the case $m = 1.035 + 0.001i$. The data was obtained by performing 100 repeated tomographic inversions when 10% multiplicative noise was added to the real and imaginary parts of the simulated complex angular scatter.

Particle size index	3.14	6.28	12.56	25.13	50.27
Retrieved refractive index	1.05	1.04	1.04	1.04	1.40
Standard deviation	<0.01	<0.01	<0.01	<0.01	0.07

The data indicate that for the first four cases where size indices = $(\pi, 2\pi, 4\pi, \text{ and } 8\pi)$ excellent values for refractive index were retrieved. In the last case where the size index was 16π , an incorrect value of 1.40 was estimated. This is due to the fact that for these larger particles, the power in scattered light is not a monotonically increasing function of refractive index. Hence, wrong values for refractive index can be obtained. Based on this, it seems clear that the retrieval of index of refraction will only be accurate for the smaller particles. Naturally, more extensive simulations would need to be done in order to gain increased confidence in a particular situation.

6. Discussion and conclusion

In this article, inversion for the Mie parameters of size index and relative refractive index have been considered via the use of tomographic inverse theory. In the case that the internal electric field in the x-component is linear in phase a straightforward relationship exists between the observed values of the scattered light field and the complex coefficients of the Fourier Transform of the internal electric field measured in the parallel scattering plane for simply polarized incident radiation. This was shown to be true for a class of low contrast particles ($m = 1.035 + .001i$) and it is not true for a class of higher contrast particles ($m = 1.58 + .001i$). Prior work, considered in [31, 32] demonstrated that under the RG approximation, the far-field scattered intensity data could be derived via Fourier theory. In this work, an analytic Mie theory is used that does not require the use of the RG approximation and is therefore applicable to a broader range of subjects.

An algorithm is proposed that uses the observed values of angular scatter to construct an equivalent spherically symmetric particle via standard tomographic inverse theory. In the case of low contrast ($m = 1.035 + .001$) the estimated size index of this new, spherically symmetric particle is close to the original one. This is true in the presence of moderate (10%) noise. Furthermore, using this estimate of size index together with a look up table from standard Mie theory, the refractive index of the particle can be inferred for a class of size indices. Here, for 4 of the 5 cases considered ($\pi, 2\pi, 4\pi, \text{ and } 8\pi$) the entire procedure

produced accurate results. In all cases of these low contrast cases, an estimate of just the size index of the particle was quite accurate.

One issue related to the implementation of the ideas presented here in an experimental system relates to the fact that it has been assumed that the complex angular scatter data is available. Although this is not common today, it can potentially be acquired via an interferometric system or by using some of the new phase sensitive optical devices.

Alternately, if only the intensity of angularly scattered data is available, these data values can be inverse transformed to obtain an estimate for the autocorrelation of the particle. This follows from the theorem that states that the Inverse Fourier Transform of the square of the Fourier Transform of an object is equal to the autocorrelation of the object [29]. The resultant real space structure could then be compared with the autocorrelation of a standard set of particles to estimate true particle size index as done above for the disk. One advantage of this idea is that it can be applied to many of the current data sets. Another option would be to utilize techniques to estimate the phase of the Fourier Transform from its modulus [33]. If these methods are successful, a complex valued angular scatter function could be inferred.

In the context of using just the intensity data for inversion, Shulman [34] demonstrated that the components of the dipole moment density correlation tensor could be obtained via inverse Fourier methods. In the case of singles particles, an estimate of particle diameter is therefore possible. However, the proposed inversion assumes that the “complete” intensity data is available as a function of wave number, something that is very difficult to measure as it requires scatter data at all wave numbers.

An additional interesting aspect of the algorithm used is that the highest wave number that is observed is $2/\lambda$. Note that information at this spatial wave number is usually unavailable in conventional microscopy. This is because in a conventional microscope, only forward scattered light is used. Examination of the Ewald sphere makes it clear that when the observed angle $|\theta| < \pi/2$ the highest observed spatial wave number is $\sqrt{2}/\lambda$. Thus, higher spatial resolution information can be obtained via the use of omni directionally scattered light.

Finally, what can be said about the general inverse for arbitrary size, shape, and refractive index via the insights gained here? Firstly, although it cannot be guaranteed, one would certainly be optimistic that such objects can be treated in a similar fashion if the relative index of refraction is low enough. However, since this article considered only the relationship between the electric field and the scattered field, values for refractive index or permittivity would need to be estimated. This is likely a more complicated problem than that considered here. Furthermore, since the internal electric field is a function of look direction, even for the spherical case considered here, the inversion cannot assume a static object. In addition, the ill-posed nature of the problem becomes apparent, especially for one viewpoint and one scattered set of angular data, as only a very small portion of Fourier Space has been acquired. The physical necessity of the solution being in conformance with Maxwell’s equations may provide a strong constraint on a given inverse or it may not. Clearly, there are many open issues that can be explored in the more general context.

Acknowledgments

The author would like to thank P. L. Roberts (UCSD), E. Boss (U. of Maine) and an anonymous reviewer for a critical review of the manuscript. Thanks are also offered to A. Lompado and C. Matzler for providing their code via on-line resources. The author is also grateful to both the Seaver Institute and the Environmental Optics and Biology program of the Office of Naval Research for supporting this work.